

See discussions, stats, and author profiles for this publication at: <https://www.researchgate.net/publication/282343749>

Stability of Osaka Mutant and Wild-Type Fibril Models

ARTICLE *in* THE JOURNAL OF PHYSICAL CHEMISTRY B · SEPTEMBER 2015

Impact Factor: 3.3 · DOI: 10.1021/acs.jpcb.5b07987

READS

27

3 AUTHORS, INCLUDING:



Workalemahu M Berhanu
University of Central Florida

37 PUBLICATIONS 291 CITATIONS

[SEE PROFILE](#)



Ulrich H E Hansmann
University of Oklahoma

213 PUBLICATIONS 4,815 CITATIONS

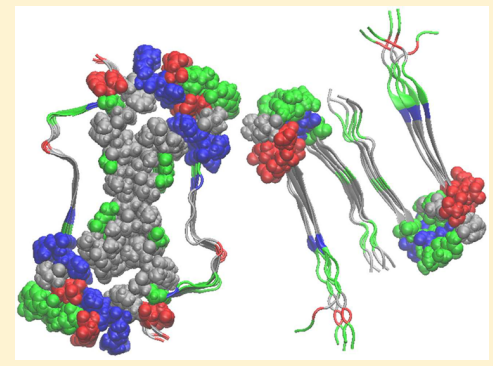
[SEE PROFILE](#)

1 Stability of Osaka Mutant and Wild-Type Fibril Models

2 Workalemahu M. Berhanu, Erik J. Alred, and Ulrich H. E. Hansmann*

3 Department of Chemistry & Biochemistry, University of Oklahoma, Norman, Oklahoma 73019, United States

4 **ABSTRACT:** Single amino acid mutations in amyloid-beta ($A\beta$) peptides can
 5 lead to early onset and increased severity of Alzheimer's disease. An example is
 6 the Osaka mutation ($A\beta_{1-40}E22D$), which is more toxic than wild-type $A\beta_{1-40}$.
 7 This mutant quickly forms early stage fibrils, one of the hallmarks of the
 8 disease, and these fibrils can even seed fibrilization of wild-type monomers.
 9 Using molecular dynamic simulations, we show that because of formation of
 10 various intra- and intermolecular salt bridges the Osaka mutant fibrils are more
 11 stable than wild-type fibrils. The mutant fibril also has a wider water channel
 12 with increased water flow than the wild type. These two observations can
 13 explain the higher toxicity and aggregation rate of the Osaka mutant over the
 14 wild type.



15 ■ INTRODUCTION

16 Protein aggregation is a factor common to various neuro-
 17 degeneration diseases, including Alzheimer's disease.¹ The
 18 latter is characterized by neuronal deposits of $A\beta$ fibrils.^{2,3}
 19 Although oligomeric aggregates seem to be the main cause for
 20 the loss of neuronal function,⁴ the thermodynamically more
 21 stable amyloid fibrils are also toxic to cell cultures.^{5,6} Likely,
 22 both $A\beta$ fibrils and oligomers cause neurodegeneration, and
 23 therefore both should be considered when therapeutic agents
 24 are developed.⁵ Amyloids form by the self-association of
 25 misfolded proteins into transient oligomers of various sizes.
 26 Once a nucleation threshold is reached, oligomers with
 27 appropriate structures become stable and act as seeds for the
 28 growth of fibrils.⁵ The end state is an equilibrium between
 29 oligomers and fibrils where dissociation and association occur
 30 continuously.⁵ *In vitro*, both oligomers and amyloid fibrils are
 31 characterized by polymorphism. For instance, at least five
 32 different structures of $A\beta_{40}$ amyloid fibrils have been
 33 determined by ssNMR, and it is expected that more will be
 34 found in the future.⁵ The differences in molecular structure
 35 between these amyloid fibril polymorphs correlate with speed
 36 of disease progress,^{7,8} and it is conjectured that these "strains"
 37 can propagate prion-like in Alzheimer patients,^{9,10} which may
 38 explain why no polymorphism is found in fibril taken from
 39 patient brains.

40 Various mutations can lead to rare familial variants of
 41 Alzheimer's disease that are characterized by early onset and/or
 42 more severe symptoms. The differences in pathogenesis are
 43 related to the higher neurotoxicity and an increase in
 44 aggregation propensity of the amyloid fibrils formed by these
 45 mutants. Hence, comparing the fibril structures of such mutants
 46 with the wild-type $A\beta$ aggregates allows one to probe the
 47 relation between fibril structure and disease progression. One
 48 example is the Osaka mutant ($\Delta E_{22}-A\beta_{1-39}$), which lacks the
 49 glutamate found in the wild type¹¹ at position 22 and rapidly
 50 forms fibrils in solution.¹² The fibril formed *in vitro* by the

Osaka mutant has a 2-fold symmetry but differs strongly in its 51
 52 quaternary structure from previously proposed fibril models of 52
 53 wild-type $A\beta_{1-40}$:⁷ instead of the simple U-shaped (hairpin) 53
 54 model of the wild-type $A\beta_{1-40}$, the Osaka structure consists of 54
 55 parallel in-register strands whose arrangement resembles a 55
 56 cinnamon roll (Figure 1). It has been suggested that this fold 56 fl
 57 could also be found for other familial mutants where the E22 57
 58 residue is not deleted but replaced by another residue located 58
 59 very close to E22⁷ of $A\beta$ wild-type sequence.⁷

Though the wild-type $A\beta_{1-40}$ fibril structures have been 60
 61 extensively studied,¹³ less is known about the energetics and the 61
 62 mechanism of aggregation of the Osaka mutant or related 62
 63 familial mutants.⁷ The missing detailed molecular level 63
 64 characterization of their structures and building principles 64
 65 may allow us to pinpoint the cause for the higher aggregation 65
 66 propensity of the Osaka mutant and the reason why preformed 66
 67 $A\beta_{1-40} E_{22}\Delta$ fibrils are very efficient in cross-seeding $A\beta$ wild- 67
 68 type aggregates, but not the other way around. Such 68
 69 characterization may also explain the higher toxicity of Osaka 69
 70 mutant. One way to probe the atomic-level structural dynamics 70
 71 and the thermodynamics of such β -sheet oligomers^{14,15} is by 71
 72 molecular dynamics simulations. Such simulations have been 72
 73 used in the past extensively to explore the structure of such 73
 74 oligomers and the pathways of their oligomerization,^{16,14} and 74
 75 they have been shown to be valuable tools for characterizing the 75
 76 structural transitions involved in $A\beta$ fibril elongation.^{17,18} In 76
 77 this paper, we utilize molecular dynamics simulations to obtain 77
 78 a deeper insight into aggregation propensity of the wild type 78
 79 and Osaka mutant and into the growth of $A\beta$ wild-type 79
 80 monomer on preformed $A\beta_{1-40} E_{22}\Delta$ nuclei. In this way, we 80
 81 hope to derive rules that may be useful for predicting structure 81
 82 of other familial mutants especially those where the mutation is 82

Received: August 17, 2015

Revised: September 23, 2015

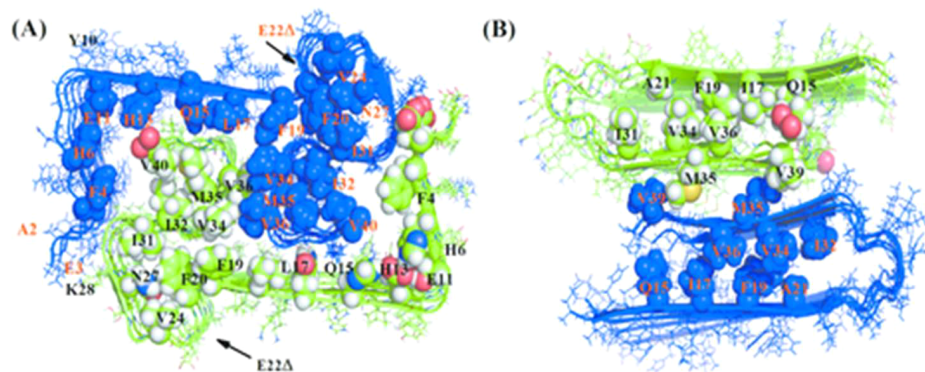


Figure 1. Comparison of the *in vitro* 2-fold symmetry ssNMR structural models of the Osaka mutant (pdb id: 2mvx) and the recent wild-type A β ₁₋₄₀ fibril. (A) The Osaka mutant model has a rectangular shape that resembles a cinnamon roll. The central part is characterized by strong hydrophobic interactions that contribute to the stability of the structure. The intermolecular salt bridge between E3 and K28 plays a significant role in maintaining its highly ordered structure. (B) The wild-type model consists of two U-shaped units with strand-loop-stand contacts L17/V36, F19/L34, A21/I32, and an intersheet contact V39/M35. The amino acid side chain contacts (interstrand and intersheet) in both models are displaced as spheres. We have colored in blue and green the two strand-loop-stand units of the double layer.

83 close the E22 (such as A β ₁₋₄₀E₂₂G [Arctic] and A β ₁₋₄₀E₂₂Q
84 [Dutch]).

85 Given current computational constraints it is not possible to
86 simulate at atomic detail directly the spontaneous fibril
87 formation of full length wild-type A β and the Osaka mutant,
88 or of the growth of wild-type A β peptides on Osaka mutant¹⁷
89 nuclei. However, information on these processes can be
90 obtained in an indirect way by contrasting the stability of Osaka
91 mutant and A β wild type, a computationally more feasible task.
92 Hence, multiple long trajectories starting from preformed wild
93 type and Osaka mutant¹⁷ fibril-like oligomer are obtained by
94 molecular dynamics simulations at constant temperature
95 simulation to evaluate the stability of wild-type and mutant
96 aggregates. These simulations will address the following
97 questions: (1) What is the role of the large number of salt
98 bridges for the structural stability the Osaka mutant fibril? (2)
99 How does the difference in the pore size affect hydration
100 dynamics and how is it related to aggregation growth and
101 toxicity? (3) How does the fibril organization (quaternary
102 structure) in the two systems leads to the observed differences
103 in seeding propensities?

104 ■ MATERIALS AND METHOD

105 **Fibril Model Construction.** The existing A β wild-type
106 fibril structures as obtained by ssNMR can be classified into
107 two forms: with a 2-fold symmetry of their quaternary structure
108 and with a 3-fold symmetry. We have shown in recent all-atom
109 explicit-solvent molecular dynamics simulations that 2-fold
110 structures are more stable.¹⁹ For this reason, we use here for
111 our wild-type A β simulations the structure recently reported by
112 Bertini et al.,²⁰ which differs slightly from earlier A β ₁₋₄₀ fibril
113 polymorphs with 2-fold symmetry in the contacts among amino
114 acid side chains within the strand-loop-strand hairpins, and
115 between these units and an additional β strand segment in the
116 N-terminal tail. We choose this model because it is the most
117 recent solid-state NMR derived experimental fibril model, and
118 because the presence of an additional N-terminal methionine in
119 well-organized fibril samples of A β 40 has led to high-resolution
120 spectra resulting in a very accurate structural model. Using this
121 model (the coordinates were kindly provided by Dr. Claudio
122 Luchinat), we build ten-layer systems by aligning two five-
123 layer systems, made each of two strand-loop-strand hairpins,

such that intersheet distances are 7.4 Å and there is a negative 124
staggering between the two β -sheet layers. For the Osaka 125
mutant we did not need to construct a model. Instead we used 126
the double-layer ten-strand structure (pdb id: 2mvx) by Schutz 127
et al.⁷ that consists of 10 strands with two β -sheets that have 128
parallel in-register strands forming a “cinnamon roll”. Note that 129
the Osaka mutant structure used in our simulation lacks the 130
staggering⁷ that has been observed in the ssNMR structure of 131
the wild-type A β .²¹ Also note that for generating these models 132
we use the first model of the respective NMR ensembles. Both 133
the Osaka mutant model and the wild-type model are shown in 134
Figure 1.

135 **Simulation Protocol.** The stability of the Osaka mutant 136
and A β wild-type decamers was probed using three 137
independent all-atom molecular dynamic simulations with an 138
AMBER ff99SB force field²² for the protein and a (TIP3P)²³ 139
model for the explicit solvent, using the GROMACS program 140
version 4.6.5-dp.²⁴ A cubic box, centered on the protein, was 141
generated with a distance from the edge of the box to the 142
protein of at least 12 Å. Because of the use of periodic 143
boundary condition we use a PME algorithm for calculation of 144
electrostatic interactions.²³ A 2 fs time step was selected, and 145
the LINCS²⁵ algorithm is used to constraint hydrogens, 146
whereas the Settle algorithm²⁶ was used for the solvent. The 147
simulations were run at a constant temperature of 310 K, 148
maintained by the Parrinello–Donadio–Bussi algorithm²⁷ ($\tau = 149$
0.1 fs),^{27,28} and the pressure of 1 bar was set with the 150
Parrinello–Rahman algorithm²⁹ ($\tau = 1$ fs).
151

152 The solvated protein is first relaxed to an energy-minimized
state; then it is equilibrated first using a NVT ensemble for 2 ns 153
and second using a pressure coupled NPT ensemble for another 154
2 ns run. Subsequently, molecular dynamics simulations of 100 155
ns are run in an NPT ensemble for both Osaka mutant and 156
wild-type A β decamers. Three separate trajectories starting 157
from different initial velocities were generated for each system. 158
Due to the use of the same initial structure, these trajectories 159
are not wholly independent, which means error estimates may 160
not be entirely realistic. Data were saved every 4 ps to allow for 161
analysis with the tools available in GROMACS. The following 162
values were measured to discern structural evolution: root- 163
means-square deviations of the C α atoms (RMSD), water 164
content within the oligomer cavity, water flow rates within the 165

166 oligomer cavity, pore diameter of the oligomer cavity,
 167 secondary structure contents, salt bridge distances (in the
 168 Osaka mutant) and hydrogen bonds. Imaging and visualization
 169 were performed using PYMOL. VMD scripts are used for
 170 analysis of the water content and flow rates.³⁰ The binding
 171 energy (in units of kcal/mol) between the two half-units of the
 172 decameric fibrils is evaluated using the MM/GBSA method
 173 implemented in AMBER 14 package.³¹

174 ■ RESULTS AND DISCUSSION

175 **Structural Stability of Osaka Mutant and Wild-Type**
A β Oligomers. One way to evaluate the stability of aggregates
 176 is by comparing the final and initial structures of a sufficiently
 177 long molecular dynamics simulation run at a physiologically
 178 relevant temperature. Visual inspection of the structures
 179 obtained after 100 ns at 310 K shows for all three trajectories
 180 little change from the initial fibril structure of the Osaka mutant
 181 oligomer (Figure 2). On the contrary, the A β wild-type

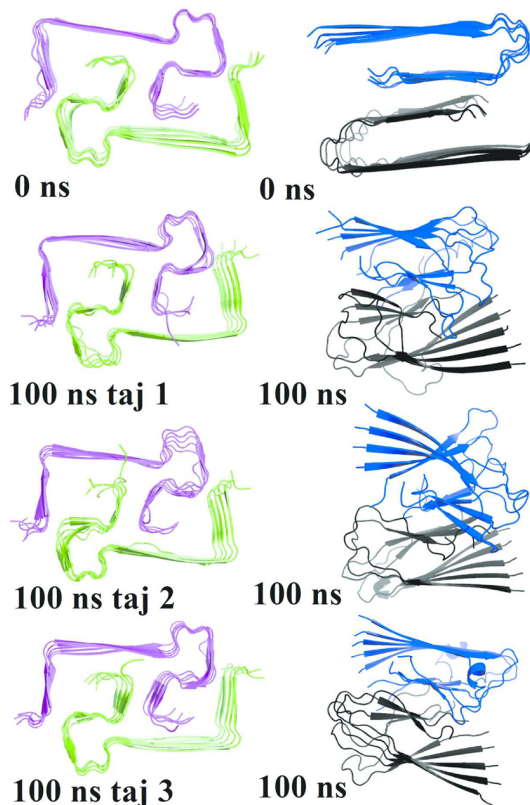


Figure 2. Snapshots of the Osaka mutant and A β wild-type fibril models at the start and end of a 100 ns molecular dynamics simulation. The 2-fold units of the Osaka mutant are magenta and green for clarification. The wild-type 2-fold units are black and blue.

183 oligomer changes along the trajectories, with the differences
 184 between final and initial structure especially pronounced in the
 185 highly flexible region of the outer chains and the turn region of
 186 the U-shaped β -sheets (Figure 2). However, despite the larger
 187 flexibility, we see no separation of monomer from the oligomers
 188 for the A β wild type. These observations are quantified by the
 189 C_{α} -RMSD (root-mean-square deviation) values between the
 190 final and initial configurations listed in (Table 1). For the
 191 rectangular-shaped two layer β -sheets of Osaka mutant
 192 decamers we find an average value of ~ 3.3 Å root-mean-

Table 1. Average C_{α} RMSD (\AA), Channel Diameter (\AA), Main Chain Hydrogen Bonds, and Average Number of Water Molecules Inside the Channel of the Osaka Mutant and Wild Type

type of analysis	run	Osaka mutant	A β wild type
C_{α} RMSD (\AA)	1	3.4	5.4
	2	3.4	5.2
	3	3.2	5.4
mean value \pm SD ^a		3.3 \pm 0.1	5.3 \pm 0.1
main chain hydrogen bonds	1	201.8	123.8
	2	196.2	122.4
	3	203.4	119.8
mean value \pm SD		200.5 \pm 3.8	122.0 \pm 2.0
pore diameter (\AA) of the first channel (1 β -sheet)	1	18.1	11.5
	2	18.4	7.6
	3	18.1	10.7
mean value \pm SD		18.2 \pm 0.2	9.9 \pm 2.1
pore diameter (\AA) of the second channel (2 β -sheet)	1	21.1	11.2
	2	20.8	12.1
	3	20.4	10.1
mean value \pm SD		20.8 \pm 0.4	11.1 \pm 1.0
av no. of water molecules in fibrils interior	1	63	17
	2	60	23
	3	60	24
mean value \pm SD		61.0 \pm 1.7	21.3 \pm 3.8
water flow (ns^{-1})	1	29.4	10.5
	2	31.2	14.3
	3	29.2	12.1
mean value \pm SD		30.0 \pm 1.1	12.3 \pm 1.9

^aMean values and standard deviation (SD) are calculated from the three values obtained by averaging over the last 25 ns of each of the three independent runs of each model.

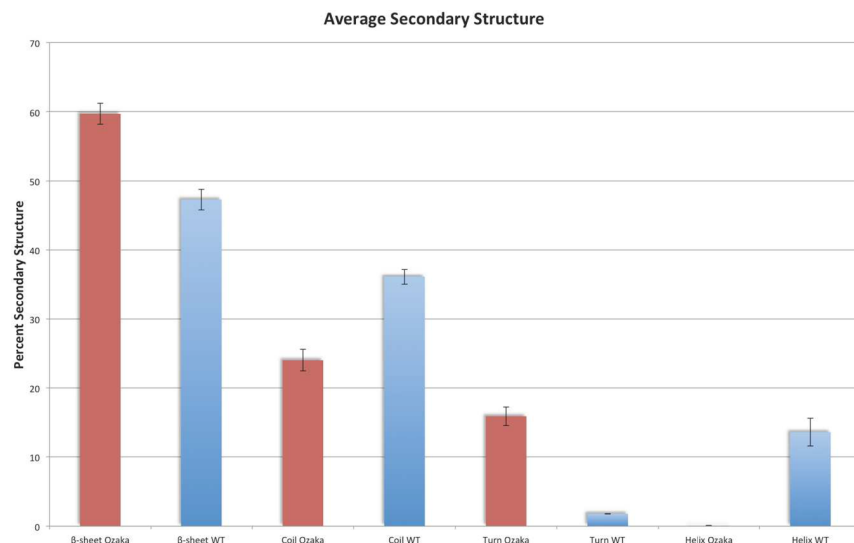
square-deviation whereas the corresponding value for A β wild-type oligomers is in the range of 5.2–5.4 Å (Table 1).

To quantify the differences in stability between Osaka mutant and wild-type A β , we compare the binding free energy of the Osaka mutant and that of the wild-type A β . This quantity describes how favorable it is to combine two smaller oligomers (of half the size) to a decamer.³² We approximate this binding energy by the MM-GBSA method as implemented in AMBER 14, using for the calculations the last 20 ns of our trajectories during which we extract 2500 snapshots separated by a time interval of 8 ps.

In terms of both accuracy and computational costs, the MM/GBSA method is halfway between empirical scoring (low cost and low accuracy) and rigorous alchemical perturbation methods (very accurate but costly). The main drawback of MM/GBSA is that the entropy term calculation is questionable due to the lack of the conformational contribution from binding-site water molecules as there is no information about how many water molecules there are in the binding site and their entropy before and after the ligand binding. There is also a problem of poor convergence of the simulated entropies.^{33,34} Despite its limitations resulting from severe approximations,³⁴ the method can be often used to reproduce and rationalize experimental findings. This is because the vibrational entropy contributes only a small fraction to the total energy³⁵ in computer simulations that model polymorphism of amyloid

Table 2. MM-PBSA-Calculated Free Energy with Its Components (kcal/mol) for Osaka Mutant and Wild Type upon Combining Two Halves of the Aggregate

system	ΔE_{vdW}	ΔE_{Ele}	ΔG_{Gb}	ΔG_{Sur}	ΔG_{Bind}
Osaka Fibril					
Traj1	-312.0	-426.6	572.4	-40.6	-206.8
Traj2	-266.7	-684.8	793.8	-38.2	-195.9
Traj3	-270.2	-386.9	515.5	-37.3	-178.9
mean value \pm SD	-283.0 \pm 25.2	-449.0 \pm 161.7	627.2 \pm 147.0	-38.7 \pm 1.7	-193.9 \pm 14.1
$\text{A}\beta$ Wt fibril					
Traj1	-166.8	-7.5	90.8	-21.4	-104.8
Traj2	-162.9	-4.7	96.4	-16.9	-87.40
Traj3	-154.9	-7.5	90.8	-21.4	-104.8
mean value \pm SD	-161.5 \pm 6.1	-6.6 \pm 1.6	93.6 \pm 3.9	-19.9 \pm 2.6	-99.0 \pm 10.0

**Figure 3.** Percentage of secondary structure of the Ozaka (red) and wild type (blue) for the last 25 ns of the simulation as predicted by DSSP and averaged between the three trajectories.

219 aggregates or the effect of single point mutants on fibril
220 stability.

221 The results of our MM/GBSA calculations in Amber 14 are
222 shown in **Table 2**. The binding energies ΔG (**Table 2**) for the
223 Osaka mutant indicate it is more structurally favorable by about
224 100 kcal/mol (~200 kcal/mol) than the wild type. The
225 energetics of both fibril oligomers is dominated by the apolar
226 terms (ΔE_{vdW} and ΔG_{sur}), especially by the vdW term. The
227 interpentameric (between the two halves of the fibril
228 oligomers) van der Waals term and the nonpolar solvation
229 terms (ΔG_{sur}) are the most significant contributions of energy
230 for the stabilization of the fibril oligomer. Binding is disfavored
231 by the electrostatic term in the solvation free energy ΔG_{GB} ,
232 whereas ΔE_{ele} , the electrostatic interaction between sheets,
233 favors binding. However, in each case, the less favorable
234 electrostatic term is offset by the nonpolar component of the
235 free energy, especially the van der Waals energy E_{vdW} as
236 opposed to the nonpolar component of solvation term (ΔG_{sur});
237 and the contribution of these two terms is higher in the Osaka
238 mutant (**Table 2**). Hence, the larger hydrophobic interaction in
239 the quaternary structure of the mutant seems to account for a
240 faster aggregation in the mutant than is seen for the wild type.
241 Note that the entropy term in our MM/GBSA calculation has
242 not been calculated, as its contribution to the total energy is
243 expected to be small, and because it can only be crudely
244 estimated. For this reason, the entropy term is, as in our case,

245 usually neglected in the determination of the relative binding
246 free energies of very similar-sized molecules.³⁶

247 In summary, visual inspection and free energy analysis of our
248 simulations suggest that the Osaka mutant forms more stable
249 nucleation units than the wild type. We note that a number of
250 previous simulations^{37,38} using a variety of force fields found
251 slightly better stability for the double-layer wild-type $\text{A}\beta$
252 reported by Tycko in 2006³⁹ than we find for the wild-type
253 model. This small difference in structural stability is likely due
254 to the slightly different intersheet and intrastrand contacts in
255 both models; however, it does not change the overall picture
256 that the Osaka mutant forms more stable nucleation units than
257 the wild type. The existence of already very stable small nuclei
258 may explain the instantaneous fibril formation that is found for
259 the Osaka mutant in *in vitro* experiments.

260 **Secondary Structure, Backbone Hydrogen Bonding, and a Dynamic Network of Salt Bridge Stabilizes the**
261 **Mutant More Than the Wild Type.** The β -sheet content and
262 the stability of amyloids are strongly correlated^{40,19} as the
263 stability of amyloid fibrils is to a large extent determined by the
264 interbackbone (main chain) hydrogen bonding network that
265 connects individual β -strands⁴¹ in the cross- β structural motif
266 common to amyloid fibrils. Such intermolecular hydrogen
267 bonding contributes about 20 times more to structural rigidity
268 than side-chain interactions between β -sheets.⁴¹ Hence, one can
269 expect that an amyloid form is the more stable, the more

271 hydrogen bonds and the higher the β -sheet content. The larger
272 average number of backbone hydrogen bonds (~200) in the
273 more stable Osaka mutant decamer as compared to the number
274 for the less stable wild-type aggregates (~122) in Table 1 is
275 consistent with this assumption.

276 Using the DSSP⁴² software, we have also compared over the
277 last 25 ns of our trajectories the secondary structure of the wild
278 types and the Osaka mutant oligomers. The Osaka mutant fibril
279 oligomers have an average β -sheet content of $60 \pm 2\%$, whereas
280 the corresponding value for the wild-type $A\beta$ oligomers is one
281 of $47 \pm 1\%$ (Figure 3). These numbers suggest that the
282 interaction between neighboring β -strands that have higher β -
283 sheet content leads for the Osaka mutant peptides to a more
284 favorable binding than seen between the wild-type chains,
285 which have a smaller β -sheet content per strand.³²

286 The Osaka mutant fibril structure⁷ is characterized by a salt
287 bridge network in the fibril core consisting of ionic intraresidue
288 interactions between H6 with E11, E11 with H13, H13 with
289 Glu11, and H13 with the V39 terminal carboxyl group (Figure
290 4). The Osaka mutant also forms an *intermolecular* salt bridge

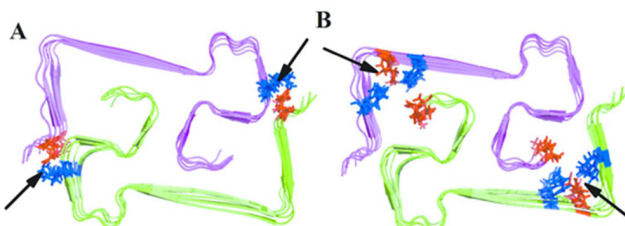


Figure 4. Salt bridge network of the Osaka mutant fibril oligomer. (A) The structure shows the intermolecular salt bridge between E3 and K28 of Osaka mutants. (B) The Osaka mutant structure has an intramolecular salt bridge consisting of three ionic intraresidue interactions between H6 with E11, E11 with H13, H13 with E11, and H13 with V39. Charged residues are red when they are negatively charged and blue when they are positively charged.

291 between E3 and K28, in which the extreme edge of N-terminal
292 residues are attached to the fibril core leading to a highly
293 ordered structure. This salt bridge may be the reason for the
294 Osaka mutant being more stable than the wild type⁷ where
295 residue K28 is part of an *intramolecular* salt bridge,⁸ and
296 therefore the N-terminus is not as tightly attached to the fibril
297 core as for the Osaka mutant.^{19,20,43} The stabilization of the N-
298 terminus via an *intermolecular* salt bridge to K28 has been
299 suggested as the key structural motif in mutants that cause early
300 onset Alzheimer disease.⁴³ Note that *intramolecular* salt
301 bridges⁸ between oppositely charged D23 and K28 side chains
302 have been found by ssNMR in wild-type $A\beta$ 40 fibril
303 polymorphs,^{8,39} but not in all polymorphs.^{39,20} For instance,
304 the structure used in our simulation does not have this salt
305 bridge. The lack of N terminal stabilization in the wild type may
306 decrease its chance to act as nucleation seed, which in turn may
307 explain why the wild type has a lower propensity for
308 aggregation than the Osaka mutant with its N-terminal
309 stabilization.^{43,44}

310 Hence, to investigate the role of such salt bridges, we have
311 analyzed the *intermolecular* salt bridge between E3 and K28 of
312 adjacent β -sheets of the Osaka mutant. This *intermolecular* salt
313 bridge can occur in the Osaka mutant between ${}_1E_n^3$ and ${}_2K_n^{28}$
314 (and ${}_2E_n^3$ and ${}_1K_n^{28}$) or between ${}_1E_n^3$ and ${}_2K_{n-1}^{28}$ (and ${}_2E_n^3$ and
315 ${}_1K_{n-1}^{28}$), where n marks for the peptide chain number, 1 stands

for the first β -sheet, 2 stands for the second β -sheet. For locating salt bridges we measure the distance between the O atom of the C=O bonds of the carboxyl group in E3 to the N atom of the NH₃⁺ group in K28. We define a *direct* salt bridges by the condition that this distance is around 4.3 Å, whereas an *indirect* or *water-mediated* salt bridge is assumed to have a distance within the range 4.3–7.0 Å.⁴⁵ We show in Figures 5

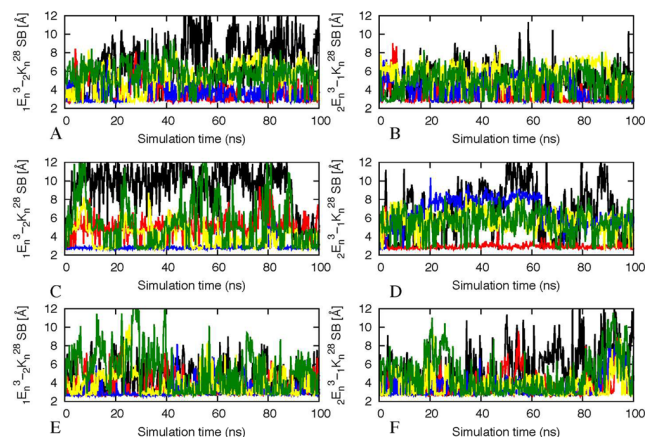


Figure 5. Average salt bridge interactions distances between ${}_1E_n^3$ and ${}_2K_n^{28}$ and ${}_2E_n^3$ and ${}_1K_n^{28}$ for the Osaka mutant. The results shown are along the 100 ns of each trajectory. Key: (A) ${}_1E_n^3$ and ${}_2K_n^{28}$ for the first run; (B) ${}_2E_n^3$ and ${}_1K_n^{28}$ for the first run; (C) ${}_1E_n^3$ and ${}_2K_n^{28}$ for the second run; (D) ${}_2E_n^3$ and ${}_1K_n^{28}$ for the second run; (E) ${}_1E_n^3$ and ${}_2K_n^{28}$ for the third run; (F) ${}_2E_n^3$ and ${}_1K_n^{28}$ for the third run. Color: black, ${}_1E_n^3$ - ${}_2K_1^{28}$; red, ${}_1E_2^3$ - ${}_2K_2^{28}$; blue, ${}_1E_3^3$ - ${}_2K_3^{28}$; green, ${}_1E_4^3$ - ${}_2K_4^{28}$; yellow, ${}_1E_5^3$ - ${}_2K_5^{28}$.

and 6 that the extended ladders of salt bridges along the interface of the N terminal E3 and the K28 of the fibril core is dynamic. For most of the trajectories, the distances are within the range 4.3–7.0 Å; hence, this salt bridge is mediated through water molecules as the E3 is on the extreme end of the N- terminus exposed to the water solvent molecules. Our results

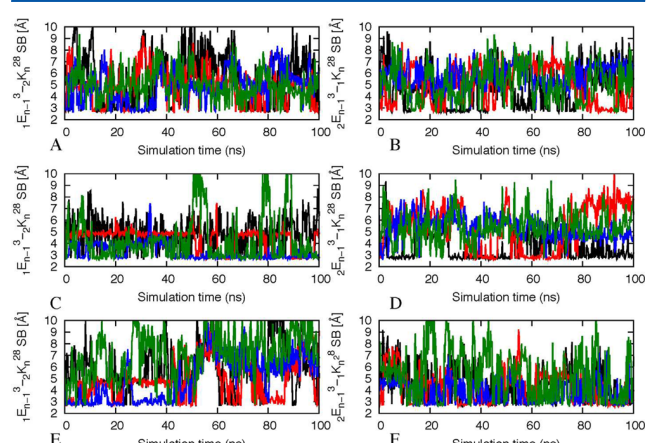


Figure 6. Average salt bridge distances between ${}_1\text{Glu}_{n-1}^3$ and ${}_2\text{Lys}_n^{28}$ and ${}_2\text{Glu}_{n-1}^3$ and ${}_1\text{Lys}_n^{28}$ of the Osaka mutant. The results are shown along the 100 ns of each trajectory. Key: (A) ${}_1E_n^3$ and ${}_2K_{n-1}^{28}$ for the first run; (B) ${}_2E_n^3$ and ${}_1K_{n-1}^{28}$ for the first run; (C) ${}_1E_n^3$ and ${}_2K_{n-1}^{28}$ for the second run; (D) ${}_2E_n^3$ and ${}_1K_{n-1}^{28}$ for the second run; (E) ${}_1E_n^3$ and ${}_2K_{n-1}^{28}$ for the third run; (F) ${}_2E_n^3$ and ${}_1K_{n-1}^{28}$ for the third run. Color: black, ${}_1E_2^3$ - ${}_2K_1^{28}$; red, ${}_1E_3^3$ - ${}_2K_2^{28}$; blue, ${}_1E_4^3$ - ${}_2K_3^{28}$; yellow, ${}_1E_5^3$ - ${}_2K_4^{28}$.

therefore support our conjecture that the salt bridge ladder at the junction between the two β -sheet units stabilizes the Osaka mutant whereas such stabilizing salt bridges are missing in the wild type. We note that our results agree with a previous study of HET-s(218–289) fungal prion fibrils that also showed the crucial role that certain salt bridges can play for the stability of aggregates.⁴⁶

Water-Mediated Entropic Forces Favor Fibril Formation for the Osaka Mutant. The NMR fibril models of both the wild-type and the Osaka mutant⁷ aggregates are characterized by a hollow core that can contain structured water forming a hydrogen-bonded network with the exposed side chains.^{19,47} However, the mutant has a cavity that is more than twice as large as that of the wild type, Table 1. This difference likely affects both the toxicity and the rate of aggregation of the two forms.

For the $A\beta$ wild type, the pore is formed by a pocket made of the A21, D23, K28, A30, I32, and L34 side chains.³⁷ We approximate the pore diameter for the first and second β -sheets by the distance between the C_α -atoms of the D23 and I32 residues of the U-shaped subunits as the distance between these two amino acids approximately corresponds to the diameter of the pore. This distance is averaged over the last 25 ns of the trajectories. For the Osaka mutant, the pore is formed by a pocket of side chains consisting of residues ⁴FRHDSGYEVH¹² and ²⁹AIIGLMVGGVV³⁹ in the adjacent U-shaped subunits. Similarly to the wild type, we define the pore size as the average of the distances distance between the C_α of H6 and M35 residues measured over the last 25 ns of the respective trajectories. Again this distance approximates well the pore diameter. We find no water molecules within the dry two-sheet interface that consists of ³¹GLMVG³⁵ residues (the dry interface results from the hydrophilic nature of this segment of Osaka mutant); however, the snapshots of $A\beta$ wild type in Figure 7 show water molecules between the two β -sheets.

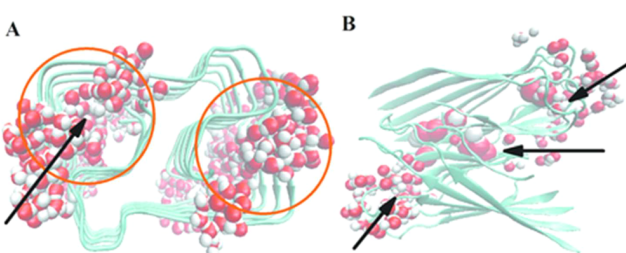


Figure 7. Wild-type $A\beta$ fibril and Osaka mutant oligomer hydration pores. The distribution of water molecules in Osaka mutant (A) and $A\beta$ fibril models within the hydrated cavity (B).

The flow of water through the pores was measured using the VMD visualization software. For this purpose, the principle axes of the oligomers are aligned with the xyz axes such that the flow of water is directed along the z axis. The z -coordinates of the center of mass of the outer pore-residues mark the vertical extension of the pore. Water molecules outside of the pore carry a tag 0, after entering from the $+z$ or $-z$ side of the pore this tag is set to +1 or -1. Exiting the pore, the tag is reset to 0; however, a permeation event requires that a water molecule with +1 (-1) tag exits the pore at the end with $-z$ ($+z$) coordinate. Hence, water molecules that enter and exit at the same side of the pore are not counted as permeation events.

The pore size of the wild type $A\beta$ fibril model averaged over three trajectories is $9.9 \pm 2.1 \text{ \AA}$ for the first β -sheet, and for the second β -sheet it is $11.1 \pm 1.0 \text{ \AA}$ (Table 1). A similar measurement for the Osaka mutant indicates a much wider inner pore diameter: for the first β -sheet the pore diameter is $18.2 \pm 0.2 \text{ \AA}$, and for the second β -sheet it is $20.8 \pm 0.4 \text{ \AA}$ (Table 1). To quantify the effect of the pore size on hydration and water mobility, we have calculated the number (averaged over the entire 100 ns simulation) of water molecules per pore, and the rate of water permeation (measured over the last 40 ns). At start, the channels of both wild type and the Osaka mutant oligomers are empty. Over the course of the simulation, surrounding bulk water moves in and fills these channels, which remain occupied by water molecules during the rest of the 100 ns simulation. The average number of water molecules (calculated as a sum of water molecules in the first and the second β -sheet) inside the Osaka mutant fibril is about 61 water molecules (Table 1) whereas only about 21 water molecules are found in the $A\beta$ wild type fibril (Table 1).

The cavity in amyloid oligomers results from the water-mediated face-to-face packing of β -sheet pairs hold together by the intermain-chain hydrogen bonding networks that are characteristic for amyloids.⁴⁸ It was found recently by a combination of neutron scattering experiments and molecular dynamic simulations that the fibril f of the τ peptide has higher diffusion coefficient and water mobility than that of the monomer.⁴⁹ This increased hydration and water mobility may promote fibril formation through an increase in the entropy of hydration water.^{49,50} This is because the association of monomers involves the release of water molecules whose distribution becomes more disordered. The resulting large gain in entropy is only partially compensated by the ordering of the peptides forming ordered interpeptide hydrogen bonds.⁵¹ In our case, the flow rate of water molecules passing through the pore in the Osaka mutant fibril oligomers is about 30 water molecules per nanosecond whereas the corresponding values for the wild type is about 12 water molecules per nanosecond (Table 1). The more than twice larger flow rate in the Osaka mutant therefore likely leads to entropic effects that encourage fibril formation,⁴⁹ similar to what has been recently shown for tau aggregation.⁵⁰

Note that the twice larger flow rate and the larger number of interior water molecules could also explain the higher toxicity of the Osaka mutant.⁵² One of the proposed mechanisms for neurotoxicity in Alzheimer's disease⁵³ is the formation of an amyloid-pore or channel in the cell membrane by $A\beta$ -aggregates. Such pores create ion channels that leads to oligomer-mediated toxicity through membrane leakage.⁵³ Hence, the presence of water molecules and their penetration into the oligomer cavity supports the cell membranes leakage mechanism of toxicity of amyloid oligomers, and the observed twice higher flow rate and number of water molecules inside the pores correlates with the Osaka mutant's higher toxicity.⁵⁴

CONCLUSION

Multiple explicit-solvent molecular dynamic simulations of the 2-fold aggregates of $A\beta$ wild type and its single residues deletion mutant E22 (Osaka mutant) were carried out to compare the wild-type with a mutant that *in vivo* is more infective and prone to aggregation. We find that Osaka mutant

438 fibrils are much more stable than wild-type fibrils, and that this
 439 difference originates from the formation of a larger number of
 440 intra- and intermolecular salt bridges in the mutant. Spirig et
 441 al.⁹ have proposed a prion-like behavior for the Osaka mutant,
 442 and $\text{A}\beta$ aggregation in general, highlighting the need for an in-
 443 depth understanding of the seeding mechanism through which
 444 Osaka mutant peptides induce $\text{A}\beta$ wild-type aggregation. Our
 445 results suggest that the more stable conformation of the Osaka
 446 mutant fibril serves as a stable nucleus for the wild-type
 447 monomers to take the unique quaternary structure of the
 448 mutant, a scenario that is consistent with the recent strain-
 449 specific traits hypothesis of Alzheimer diseases. The underlying
 450 idea that the wild-type monomers are flexible and assume their
 451 structure depending on interaction with environment and other
 452 molecules is also in agreement with the existence of various of
 453 polymorphic forms observed previously including most
 454 interestingly the 3-fold conformation recently reported
 455 Nussinov and co-workers.⁵⁵

456 In addition to its higher stability, the Osaka mutant fibril also
 457 has a wider hydration channel that may play a significant role
 458 for its toxicity and aggregation. The wider hollow channel in
 459 the Osaka mutant is hydrated as in the wild type but the rate of
 460 flow of water is more than 2-fold for the mutant. The larger
 461 hydration rate and expulsion of the water molecules could
 462 promote formation of fibers by increasing hydration water
 463 entropy when compared to the similar-sized oligomer. The
 464 observed difference in water penetrating of the mutant and wild
 465 type can explain the experimentally observed differences in
 466 toxicity if one assumes pore formation and membrane leakage
 467 as toxicity mechanism.

468 ■ AUTHOR INFORMATION

469 Corresponding Author

470 *E-mail: uhansmann@ou.edu.

471 Notes

472 The authors declare no competing financial interest.

473 ■ ACKNOWLEDGMENTS

474 We thank Dr. Claudio Luchinat for providing the atomic
 475 coordinates of the $\text{A}\beta$ 40 fibril models. This work used
 476 resources of the National Energy Research Scientific Comput-
 477 ing Center, which is supported by the Office of Science of the
 478 U.S. Department of Energy under contract no. DE-AC02-
 479 05CH11231. Other parts of the simulations were done on the
 480 BOOMER cluster of the University of Oklahoma. We
 481 acknowledge financial support from NSF CHE-1266256 and
 482 OCAST HR14-129.

483 ■ REFERENCES

- 484 (1) Eisenberg, D.; Jucker, M. The Amyloid State of Proteins in
 485 Human Diseases. *Cell* **2012**, *148*, 1188–1203.
- 486 (2) Nasica-Labouze, J.; Nguyen, P. H.; Sterpone, F.; Berthoumieu,
 487 O.; Buchete, N. V.; Coté, S.; De Simone, A.; Doig, A. J.; Faller, P.;
 488 Garcia, A.; et al. Amyloid Beta Protein and Alzheimer's Disease: When
 489 Computer Simulations Complement Experimental Studies. *Chem. Rev.*
 490 **2015**, *115*, 3518–3563.
- 491 (3) Blennow, K.; de Leon, M. J.; Zetterberg, H. Alzheimer's Disease.
 492 *Lancet* **2006**, *368*, 387–403.
- 493 (4) Shankar, G. M.; Li, S. M.; Mehta, T. H.; Garcia-Munoz, A.;
 494 Shepardson, N. E.; Smith, I.; Brett, F. M.; Farrell, M. A.; Rowan, M. J.;
 495 Lemere, C. A.; et al. Amyloid-Beta Protein Dimers Isolated Directly
 496 from Alzheimer's Brains Impair Synaptic Plasticity and Memory. *Nat.*
 497 *Med.* **2008**, *14*, 837–842.

- (5) Tycko, R. Amyloid Polymorphism: Structural Basis and 498 Neurobiological Relevance. *Neuron* **2015**, *86*, 632–645. 499
- (6) Qiang, W.; Yau, W. M.; Luo, Y. Q.; Mattson, M. P.; Tycko, R. 500 Antiparallel Beta-Sheet Architecture in Iowa-Mutant Beta-Amyloid 501 Fibrils. *Proc. Natl. Acad. Sci. U. S. A.* **2012**, *109*, 4443–4448. 502
- (7) Schutz, A. K.; Vagt, T.; Huber, M.; Ovchinnikova, O. Y.; Cadalbert, R.; Wall, J.; Guntert, P.; Bockmann, A.; Glockshuber, R.; Meier, B. H. Atomic-Resolution Three-Dimensional Structure of 505 Amyloid Beta Fibrils Bearing the Osaka Mutation. *Angew. Chem., Int. 506 Ed.* **2015**, *54*, 331–335. 507
- (8) Lu, J. X.; Qiang, W.; Yau, W. M.; Schwieters, C. D.; Meredith, S. C.; Tycko, R. Molecular Structure of Beta-Amyloid Fibrils in 508 Alzheimer's Disease Brain Tissue. *Cell* **2013**, *154*, 1257–1268. 509
- (9) Spirig, T.; Ovchinnikova, O.; Vagt, T.; Glockshuber, R. Direct 510 Evidence for Self-Propagation Different Amyloid-Beta Fibril Con- 511 formations. *Neurodegener. Dis.* **2014**, *14*, 151–159. 512
- (10) Stohr, J.; Watts, J. C.; Mensinger, Z. L.; Oehler, A.; Grillo, S. K.; DeArmond, S. J.; Prusiner, S. B.; Giles, K. Purified and Synthetic 515 Alzheimer's Amyloid Beta ($\text{A}\beta$) Prions. *Proc. Natl. Acad. Sci. U. S. A.* **2012**, *109*, 11025–11030. 517
- (11) Tomiyama, T.; Matsuyama, S.; Iso, H.; Umeda, T.; Takuma, H.; Ohnishi, K.; Ishibashi, K.; Teraoka, R.; Sakama, N.; Yamashita, T.; et al. A Mouse Model of Amyloid Beta Oligomers: Their Contribution 520 to Synaptic Alteration, Abnormal Tau Phosphorylation, Glial 521 Activation, and Neuronal Loss in Vivo. *J. Neurosci.* **2010**, *30*, 4845– 522 4856. 523
- (12) Cloe, A. L.; Orgel, J.; Sachleben, J. R.; Tycko, R.; Meredith, S. C. 524 The Japanese Mutant $\text{A}\beta$ ($\Delta\text{E22-A}\beta(1-39)$) Forms Fibrils Instanta- 525 neously, with Low-Thioflavin T Fluorescence: Seeding of Wild-Type 526 $\text{A}\beta$ (1–40) into Atypical Fibrils by $\Delta\text{E22-A}\beta(1-39)$. *Biochemistry* **2011**, *50*, 2026–2039. 527
- (13) Takeda, T.; Klimov, D. K. Replica Exchange Simulations of the 529 Thermodynamics of Abeta Fibril Growth. *Biophys. J.* **2009**, *96*, 442– 530 52.
- (14) Blinov, N.; Dorosh, L.; Wishart, D.; Kovalenko, A. Association 532 Thermodynamics and Conformational Stability of Beta-Sheet Amyloid 533 Beta(17–42) Oligomers: Effects of E22Q (Dutch) Mutation and 534 Charge Neutralization. *Biophys. J.* **2010**, *98*, 282–296. 535
- (15) Berhanu, W. M.; Hansmann, U. H. E. In *Biomolecular Modelling 536 and Simulations*; Karabencheva-Christova, T., Ed.; Elsevier Academic 537 Press Inc.: San Diego, 2014; Vol. 96, pp 113–141. 538
- (16) Ma, B. Y.; Nussinov, R. Simulations as Analytical Tools to 539 Understand Protein Aggregation and Predict Amyloid Conformation. 540 *Curr. Opin. Chem. Biol.* **2006**, *10*, 445–452. 541
- (17) Han, W.; Schulten, K. Fibril Elongation by $\text{A}\beta(17-42)$: Kinetic 542 Network Analysis of Hybrid-Resolution Molecular Dynamics Simu- 543 lations. *J. Am. Chem. Soc.* **2014**, *136*, 12450–12460. 544
- (18) Cheon, M.; Hall, C. K.; Chang, I. Structural Conversion of $\text{A}\beta$ 545 17–42 Peptides from Disordered Oligomers to U-Shape Protofila- 546 ments Via Multiple Kinetic Pathways. *PLoS Comput. Biol.* **2015**, *11*, 547 e1004258. 548
- (19) Alred, E. J.; Phillips, M.; Berhanu, W. M.; Hansmann, U. H. E. 549 On the Lack of Polymorphism in $\text{A}\beta$ -Peptide Aggregates Derived from 550 Patient Brains. *Protein Sci.* **2015**, *24*, 923–935. 551
- (20) Bertini, I.; Gonnelli, L.; Luchinat, C.; Mao, J. F.; Nesi, A. A New 552 Structural Model of A Beta(40) Fibrils. *J. Am. Chem. Soc.* **2011**, *133*, 553 16013–16022. 554
- (21) GhattyVenkataKrishna, P. K.; Überbacher, E. C.; Cheng, X. L. 555 Effect of the Amyloid Beta Hairpin's Structure on the Handedness of 556 Helices Formed by Its Aggregates. *FEBS Lett.* **2013**, *587*, 2649–2655. 557
- (22) Hornak, V.; Abel, R.; Okur, A.; Strockbine, B.; Roitberg, A.; 558 Simmerling, C. Comparison of Multiple Amber Force Fields and 559 Development of Improved Protein Backbone Parameters. *Proteins: 560 Struct., Funct., Genet.* **2006**, *65*, 712–725. 561
- (23) Jorgensen, W. L.; Chandrasekhar, J.; Madura, J. D.; Impey, R. 562 W.; Klein, M. L. Comparison of Simple Potential Functions for 563 Simulating Liquid Water. *J. Chem. Phys.* **1983**, *79*, 926–935. 564
- (24) Pronk, S.; Pall, S.; Schulz, R.; Larsson, P.; Bjelkmar, P.; 565 Apostolov, R.; Shirts, M. R.; Smith, J. C.; Kasson, P. M.; van der Spoel, 566

- 567 D.; et al. Gromacs 4.5: A High-Throughput and Highly Parallel Open
568 Source Molecular Simulation Toolkit. *Bioinformatics* **2013**, *29*, 845–
569 854.
- 570 (25) Hess, B. P-Lincs: A Parallel Linear Constraint Solver for
571 Molecular Simulation. *J. Chem. Theory Comput.* **2008**, *4*, 116–122.
- 572 (26) Miyamoto, S.; Kollman, P. A. Settle - an Analytical Version of
573 the Shake and Rattle Algorithm for Rigid Water Models. *J. Comput.*
574 *Chem.* **1992**, *13*, 952–962.
- 575 (27) Bussi, G.; Donadio, D.; Parrinello, M. Canonical Sampling
576 through Velocity Rescaling. *J. Chem. Phys.* **2007**, *126*, 014101.
- 577 (28) Bussi, G.; Zykova-Timan, T.; Parrinello, M. Isothermal-Isobaric
578 Molecular Dynamics Using Stochastic Velocity Rescaling. *J. Chem.*
579 *Phys.* **2009**, *130*, 074101.
- 580 (29) Parrinello, M.; Rahman, A. Polymorphic Transitions in Single-
581 Crystals - a New Molecular-Dynamics Method. *J. Appl. Phys.* **1981**, *52*,
582 7182–7190.
- 583 (30) Humphrey, W.; Dalke, A.; Schulten, K. Vmd: Visual Molecular
584 Dynamics. *J. Mol. Graphics* **1996**, *14*, 33–38.
- 585 (31) Case, D. A.; Cheatham, T. E.; Darden, T.; Gohlke, H.; Luo, R.;
586 Merz, K. M.; Onufriev, A.; Simmerling, C.; Wang, B.; Woods, R. J. The
587 Amber Biomolecular Simulation Programs. *J. Comput. Chem.* **2005**, *26*,
588 1668–1688.
- 589 (32) Auer, S. Nucleation of Polymorphic Amyloid Fibrils. *Biophys. J.*
590 **2015**, *108*, 1176–1186.
- 591 (33) Genheden, S.; Ryde, U. Will Molecular Dynamics Simulations
592 of Proteins Ever Reach Equilibrium? *Phys. Chem. Chem. Phys.* **2012**, *14*,
593 8662–8677.
- 594 (34) Genheden, S.; Ryde, U. The Mm/Pbsa and Mm/Gbsa Methods
595 to Estimate Ligand-Binding Affinities. *Expert Opin. Drug Discovery*
596 **2015**, *10*, 449–461.
- 597 (35) Park, J.; Kahng, B.; Hwang, W. Thermodynamic Selection of
598 Steric Zipper Patterns in the Amyloid Cross-Beta Spine. *PLoS Comput.*
599 *Biol.* **2009**, *5*, e1000492.
- 600 (36) Homeyer, N.; Gohlke, H. Free Energy Calculations by the
601 Molecular Mechanics Poisson-Boltzmann Surface Area Method. *Mol.*
602 *Inf.* **2012**, *31*, 114–122.
- 603 (37) Zheng, J.; Jang, H.; Ma, B.; Tsai, C. J.; Nussinov, R. Modeling
604 the Alzheimer a Beta(17–42) Fibril Architecture: Tight Intermolecular
605 Sheet-Sheet Association and Intramolecular Hydrated Cavities.
606 *Biophys. J.* **2007**, *93*, 3046–3057.
- 607 (38) Kahler, A.; Sticht, H.; Horn, A. H. Conformational Stability of
608 Fibrillar Amyloid-Beta Oligomers Via Protofilament Pair Formation - a
609 Systematic Computational Study. *PLoS One* **2013**, *8*, e70521.
- 610 (39) Petkova, A. T.; Yau, W. M.; Tycko, R. Experimental Constraints
611 on Quaternary Structure in Alzheimer's Beta-Amyloid Fibrils.
612 *Biochemistry* **2006**, *45*, 498–512.
- 613 (40) Shammas, S. L.; Knowles, T. P. J.; Baldwin, A. J.; MacPhee, C.
614 E.; Welland, M. E.; Dobson, C. M.; Devlin, G. L. Perturbation of the
615 Stability of Amyloid Fibrils through Alteration of Electrostatic
616 Interactions. *Biophys. J.* **2011**, *100*, 2783–2791.
- 617 (41) Fitzpatrick, A. W. P.; Vanacore, G. M.; Zewail, A. H.
618 Nanomechanics and Intermolecular Forces of Amyloid Revealed by
619 Four-Dimensional Electron Microscopy. *Proc. Natl. Acad. Sci. U. S. A.*
620 **2015**, *112*, 3380–3385.
- 621 (42) Kabsch, W.; Sander, C. Dictionary of Protein Secondary
622 Structure - Pattern-Recognition of Hydrogen-Bonded and Geometrical
623 Features. *Biopolymers* **1983**, *22*, 2577–2637.
- 624 (43) Schledorn, M.; Meier, B. H.; Böckmann, A. Alternative Salt
625 Bridge Formation in $\text{A}\beta$ - a Hallmark of Early-Onset Alzheimer's
626 Disease? *Front. Mol. Biosci.* **2015**, *2*, 2.
- 627 (44) Meier, B. H.; Böckmann, A. The Structure of Fibrils from
628 'Misfolded' Proteins. *Curr. Opin. Struct. Biol.* **2015**, *30*, 43–49.
- 629 (45) Berhanu, W. M.; Hansmann, U. H. E. Structure and Dynamics
630 of Amyloid-Beta Segmental Polymorphisms. *PLoS One* **2012**, *7*,
631 e41479.
- 632 (46) Lange, A.; Gattin, Z.; Van Melckebeke, H.; Wasmer, C.; Soragni,
633 A.; van Gunsteren, W. F.; Meier, B. H. A Combined Solid-State Nmr
634 and Md Characterization of the Stability and Dynamics of the Het-
- S(218–289) Prion in Its Amyloid Conformation. *ChemBioChem* **2009**, *10*, 1657–1665.
- (47) Fitzpatrick, A. W. P.; Debouchina, G. T.; Bayro, M. J.; Clare, D. K.; Caporini, M. A.; Bajaj, V. S.; Jaroniec, C. P.; Wang, L. C.; Ladizhansky, V.; Muller, S. A.; et al. Atomic Structure and Hierarchical Assembly of a Cross-Beta Amyloid Fibril. *Proc. Natl. Acad. Sci. U. S. A.* **2013**, *110*, 5468–5473.
- (48) Chen, S. W.; Drakulic, S.; Deas, E.; Ouberai, M.; Aprile, F. A.; Arranz, R.; Ness, S.; Roodveldt, C.; Guilliams, T.; De-Genst, E. J.; et al. Structural Characterization of Toxic Oligomers That Are Kinetically Trapped During Alpha-Synuclein Fibril Formation. *Proc. Natl. Acad. Sci. U. S. A.* **2015**, *112*, E1994–E2003.
- (49) Fichou, Y.; Schiro, G.; Gallat, F. X.; Laguri, C.; Moulin, M.; Combete, J.; Zamponi, M.; Hartlein, M.; Picart, C.; Mossou, E.; et al. Hydration Water Mobility Is Enhanced around Tau Amyloid Fibers. *Proc. Natl. Acad. Sci. U. S. A.* **2015**, *112*, 6365–6370.
- (50) Sun, T. J.; Lin, F. H.; Campbell, R. L.; Allingham, J. S.; Davies, P. L. An Antifreeze Protein Folds with an Interior Network of More Than 400 Semi-Clathrate Waters. *Science* **2014**, *343*, 795–798.
- (51) Thirumalai, D.; Reddy, G.; Straub, J. E. Role of Water in Protein Aggregation and Amyloid Polymorphism. *Acc. Chem. Res.* **2012**, *45*, 83–92.
- (52) Ovchinnikova, O. Y.; Finder, V. H.; Vodopivec, I.; Nitsch, R. M.; Glockshuber, R. The Osaka Fad Mutation E22 Δ Leads to the Formation of a Previously Unknown Type of Amyloid- β Fibrils and Modulates $\text{A}\beta$ Neurotoxicity. *J. Mol. Biol.* **2011**, *408*, 780–791.
- (53) Quist, A.; Doudevski, L.; Lin, H.; Azimova, R.; Ng, D.; Frangione, B.; Kagan, B.; Ghiso, J.; Lal, R. Amyloid Ion Channels: A Common Structural Link for Protein-Misfolding Disease. *Proc. Natl. Acad. Sci. U. S. A.* **2005**, *102*, 10427–10432.
- (54) Lashuel, H. A.; Hartley, D.; Petre, B. M.; Walz, T.; Lansbury, P. T. Neurodegenerative Disease - Amyloid Pores from Pathogenic Mutations. *Nature* **2002**, *418*, 291–291.
- (55) Xiao, Y. L.; Ma, B. Y.; McElheny, D.; Parthasarathy, S.; Long, F.; Hoshi, M.; Nussinov, R.; Ishii, Y. $\text{A}\beta(1–42)$ Fibril Structure Illuminates Self-Recognition and Replication of Amyloid in Alzheimer's Disease. *Nat. Struct. Mol. Biol.* **2015**, *22*, 499–505.